The Hydraulics of an Evolving Upwelling Jet Flowing around a Cape

ANDREW C. DALE AND JOHN A. BARTH

College of Oceanic and Atmospheric Sciences, Oregon State University, Corvallis, Oregon

ABSTRACT

Upwelling jets flow alongshore in approximate geostrophic balance with the onshore pressure gradient induced by coastal upwelling. Observations of such jets have shown that they often move offshore downstream of capes, leaving a pool of upwelled water inshore. Comparisons are made between this behavior and the hydraulic transition of a potential-vorticity-conserving coastal current as it passes a topographic anomaly at which it is exactly critical to long coastal-trapped waves. An analytic 1.5-layer model of coastal hydraulics with constant potential vorticity in each layer predicts flow fields (i.e., jet separation) in critical situations that resemble observations. When scales approximate Cape Blanco on the Oregon coast, separation occurs at a jet transport of around 0.76×10^6 m³ s⁻¹, similar to observed transports. Time-dependent, semigeostrophic calculations suggest that, during an upwelling season, the jet would evolve from a weak flow, which was subcritical everywhere and symmetric about the cape, to an exactly critical state that made a transition from subcritical to supercritical structure at the head of the cape. The predicted flow field at critical transition consists of a narrow upwelling jet upstream of the cape that moves offshore and broadens at the cape. This critical state would be accompanied by a downstream jump back to subcritical conditions. Further upwelling-favorable winds would lead to transient waves that propagated upstream and downstream, modifying the upstream and downstream conditions and restoring criticality. Thus, the head of the cape exerts hydraulic control on the flow and prevents the jet transport from increasing above its critical level.

Inherent in the hydraulic approach is the assumption that alongshore scales are large. For realistic alongshore scales, solutions modified by coastline curvature suggest that the convexity of the head of a cape slightly inhibits the transition to a strongly upwelled downstream state by increasing the required critical transport. In the presence of topographic features with finite alongshore scale, the hydraulic approach can be used to construct a flow field, although this flow field has an inherent error arising from the implicit assumptions regarding scales. Estimation of this error for topography representing Cape Blanco suggests that in places the cape is rather abrupt for hydraulic theory to be valid.

1. Introduction

When upwelling occurs in a coastal region, it sets up an alongshore inertial jet. Such jets tend to move offshore downstream of capes (e.g., Kelly 1985), leaving a pool of dense upwelled water inshore. It is clear from sea surface temperature images (e.g., Fig. 1) that these features are common in upwelling regions, with important implications for the transport of shelf water to the deep ocean (Barth and Smith 1998; Barth et al. 2000). That the transition in behavior occurs at a topographic anomaly (the cape) is suggestive of a hydraulic process, although no link has previously been made with the existing literature on coastal hydraulics.

Hydraulics describes the evolution along streamlines of a steady flow as it encounters gradual changes in its environment. This evolution is governed by the conserved quantities of the flow. Coastal hydraulics concerns currents that flow parallel to a coastline, encountering topography (a term that here includes both bottom bathymetry and coastline orientation) that changes gradually alongshore. The structure of the current (in a vertical section) adjusts to accommodate changes in topography and latitude but always conserves its total transport and potential vorticity distribution. When, for a given topography, two or more distinct current structures have identical transport and potential vorticity distributions, they are termed "conjugate" structures (Gill and Schumann 1979, henceforth GS79). As a coastal current encounters a localized topographic anomaly (such as a narrowing of the shelf), GS79 proposed that its structure can distort smoothly from one structure to its conjugate, resulting in a flow field that is asymmetric about the topographic feature. A smooth transition can occur only if the two conjugate structures are identical at the point where the anomaly is most pronounced. At such a point the current is exactly critical to long coastal-trapped waves, stalling their upstream propagation. Up-

Corresponding author address: Dr. Andrew C. Dale, College of Oceanic and Atmospheric Sciences, Oregon State University, 104 Ocean Admin. Building, Corvallis, OR 97331-5503.
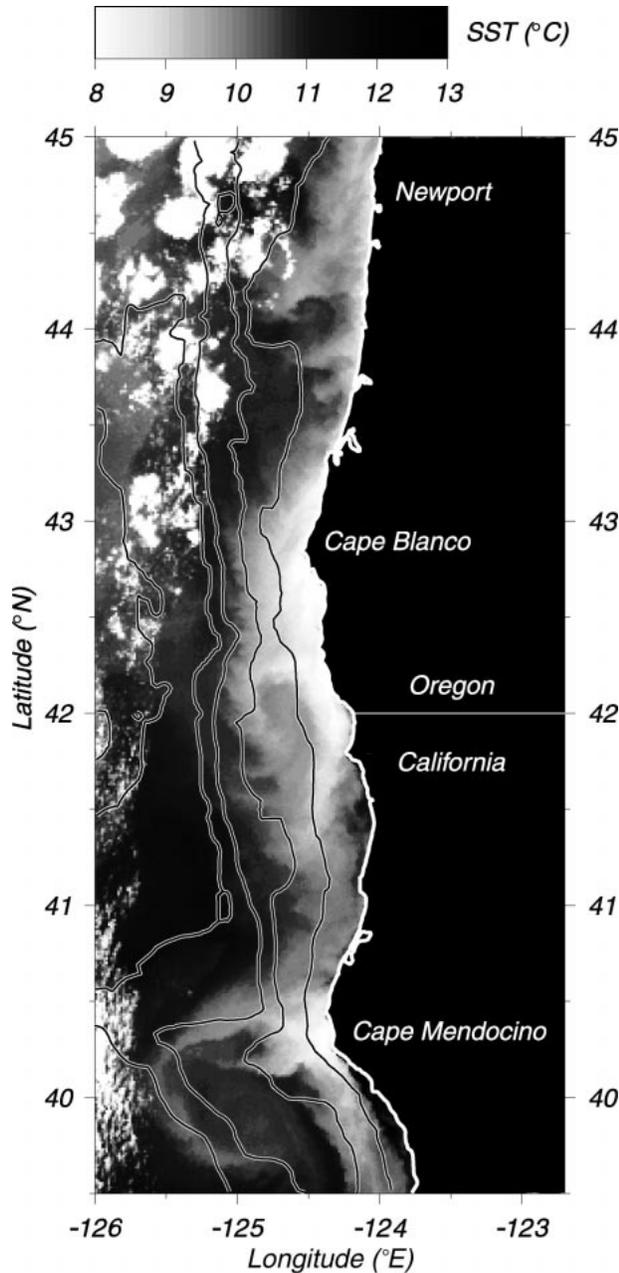E-mail: acd@oce.orst.edu

FIG. 1. Sea surface temperature from 18 May 1995 at 2100 UTC for a region of the U.S. west coast. Isobaths are shown at 200 m (approximates the shelf edge), 1000 m, 2000 m, and 3000 m.

stream and downstream conditions are subcritical and supercritical, respectively.

"Hydraulic control" occurs when a flow adjusts (in time) to an eventual steady state in which it makes a smooth transition of structure. The critical point at which the transition occurs is then known as the "control point." Adjustment of the flow is achieved through "upstream influence" in which the nature of the control point is communicated to the subcritical flow upstream by nonlinear waves, which modify the upstream state

(Long 1972). The final steady state thus depends crucially on the nature of the control point. An upwelling jet evolves in strength as the upwelling season progresses, increasing the likelihood that it is at some time exactly critical and able to smoothly transition between conjugate structures. The interesting possibility that hydraulic control may then limit jet transport by preserving criticality once it is established will be discussed later.

Several other mechanisms have been proposed as explanations for the enhanced upwelling observed in the lee of capes. These include the variation in wind stress due to the change in angle of the coastline and/or land topography (Kelly 1985), variations in bottom topography (Peffley and O'Brien 1976), and inability of the jet to adjust to rapidly varying topography, such as in the inertial "overshoot" of a strong jet. This paper investigates the proposed hydraulic mechanism through application of a simple model of coastal hydraulics governed by shelf width (an extension of GS79), with the added complication of an upstream state that evolves in time. Initially only steady states, representative of the evolving upwelling system at particular times, are considered, with the simplest case having long alongshore scales (section 3). Finite alongshore topographic scales both violate the underlying assumptions of hydraulics and imply curvature of the coastline and/or bathymetry, a factor which alone can lead to the separation of a jet from a coastline (Ou and de Ruijter 1986). A modified GS79 model allows investigation of the effect of curvature on the conditions required for criticality at the head of a cape (section 4). In section 5, an approximation to the topography of Cape Blanco is used to construct a critical solution, allowing an assessment of the relevance of the scales of the problem in a realistic case. The validity of the hydraulic approach for finite alongshore scales is also examined. Finally, in section 6, time-dependent solutions provide insight into the evolution of the system when it is subject to continuous upwelling. A hydraulically controlled state is established with critical conditions at the head of the cape.

2. Formulation

Consider a two-layer system in which the ith layer, of density ρ_i, has thickness h_i and velocity components u_i, v_i in the x, y directions, respectively. The surface is capped by a rigid lid on which the pressure is $\Phi(x, y)$. Hydrostatic, Boussinesq equations of motion for the two layers ($i = 1, 2$) are then

$$\frac{Du_i}{Dt} - fv_i = -\frac{\partial p_i}{\partial x}, \tag{1}$$

$$\frac{Dv_i}{Dt} + fu_i = -\frac{\partial p_i}{\partial y}, \quad \text{and} \tag{2}$$

$$\frac{Dh_i}{Dt} = -h_i\left(\frac{\partial u_i}{\partial x} + \frac{\partial v_i}{\partial y}\right), \tag{3}$$
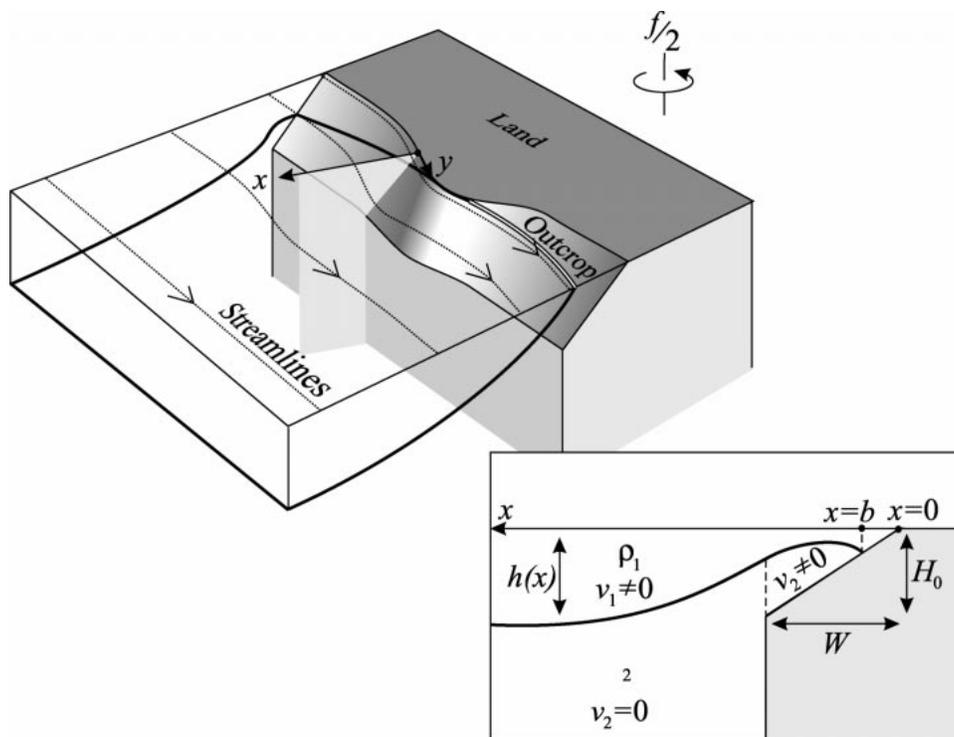
FIG. 2. A schematic view of a two-layer coastal ocean with an alongshore current in the upper layer flowing past a cape where there is a constriction and steepening of the shelf. The insert shows a vertical cross-shore section.

where $D/Dt = \partial/\partial t + u_i \partial/\partial x + v_i \partial/\partial y$, f is the Coriolis parameter, $p_1 = \Phi/\rho_0$, $p_2 = p_1 - g'h_1$, ρ_0 is a representative density, and $g' = g(\rho_2 - \rho_1)/\rho_0$ is the reduced gravity. Standard manipulations of (1), (2), and (3) show that potential vorticity

$$\Pi_i = \frac{f + \partial v_i/\partial x - \partial u_i/\partial y}{h_i} \qquad (4)$$

is conserved along streamlines ($D\Pi_i/Dt = 0$), as is the Bernoulli function

$$B_i = p_i + \frac{1}{2}(u_i^2 + v_i^2) \qquad (5)$$

when flow is steady ($\partial/\partial t = 0$).

a. Slowly varying coastal jet

In the configuration of Fig. 2, a slowly varying jet flows along a curved coastline. We rotate axes such that locally the x axis points offshore and the y axis points alongshore opposite to the direction of coastal-trapped wave propagation. Since the coastline may be curved, such a coordinate system is curvilinear. Equations (1), (2), and (4) transform to

$$\frac{\partial u_i}{\partial t} + u_i \frac{\partial u_i}{\partial x} + \left(\frac{R}{R + x}\right) v_i \frac{\partial u_i}{\partial y} - \frac{v_i^2}{R + x} - fv_i$$
$$= -\frac{\partial p_i}{\partial x}, \qquad (6)$$

$$\frac{\partial v_i}{\partial t} + u_i \frac{\partial v_i}{\partial x} + \left(\frac{R}{R + x}\right) v_i \frac{\partial v_i}{\partial y} + \frac{u_i v_i}{R + x} + fu_i$$
$$= -\left(\frac{R}{R + x}\right) \frac{\partial p_i}{\partial y}, \qquad (7)$$

and

$$\Pi_i = \left[f + \frac{\partial v_i}{\partial x} - \left(\frac{R}{R + x}\right) \frac{\partial u_i}{\partial y} + \frac{v_i}{R + x} \right] \Big/ h_i, \quad (8)$$

where $R(y)$ is the radius of curvature of the coastline. Equation (5) is unchanged. The alongshore variation of R is assumed to be gradual and is neglected.

The problem is nondimensionalized with respect to the scales h_∞, a, L, U, V, $a^2 f^2$, and f/h_∞ for vertical distance, offshore distance, alongshore distance, offshore velocity, alongshore velocity, pressure/density, and potential vorticity, respectively. Here $a = \sqrt{g'h_\infty}/f$ is the internal Rossby radius of deformation and $h_\infty =$

$\lim_{x\to\infty} h_1(x)$ is the depth of the layer interface far offshore. There will be no change of notation to signify nondimensional variables since they will be used exclusively from this point onward.

If the alongshore velocity is largely geostrophic, an appropriate choice for the scale V is af. Continuity considerations (Roed 1980) relate the alongshore and offshore scalings through

$$UL = Va, \tag{9}$$

so $U = a^2f/L$. Time is scaled by the advective timescale $L/V = a/U = L/(af)$. Equations (6)–(8) and (5) become

$$\left(\frac{a}{L}\right)^2 \frac{\partial u_i}{\partial t} + \left(\frac{a}{L}\right)^2 u_i \frac{\partial u_i}{\partial x} + \left(\frac{a}{L}\right)^2 \left(\frac{R}{R+x}\right) v_i \frac{\partial u_i}{\partial y} - \frac{v_i^2}{R+x} - v_i = -\frac{\partial p_i}{\partial x}, \tag{10}$$

$$\frac{\partial v_i}{\partial t} + u_i \frac{\partial v_i}{\partial x} + \left(\frac{R}{R+x}\right) v_i \frac{\partial v_i}{\partial y} + \frac{u_i v_i}{R+x} + u_i = -\left(\frac{R}{R+x}\right) \frac{\partial p_i}{\partial y}, \tag{11}$$

$$\Pi_i = \left[1 + \frac{\partial v_i}{\partial x} - \left(\frac{a}{L}\right)^2 \left(\frac{R}{R+x}\right) \frac{\partial u_i}{\partial y} + \frac{v_i}{R+x}\right] \Big/ h_i, \quad \text{and} \tag{12}$$

$$B_i = p_i + \frac{1}{2}\left[\left(\frac{a}{L}\right)^2 u_i^2 + v_i^2\right]. \tag{13}$$

Appealing to the standard assumption of hydraulics-type problems, that variation along the flow is gradual compared to variation across the flow ($a/L \ll 1$),

$$\frac{v_i^2}{R+x} + v_i = \frac{\partial p_i}{\partial x}, \tag{14}$$

$$\frac{\partial v_i}{\partial t} + \left(\frac{R}{R+x}\right) v_i \frac{\partial v_i}{\partial y} + u_i \Pi_i h_i = -\left(\frac{R}{R+x}\right) \frac{\partial p_i}{\partial y}, \tag{15}$$

$$\Pi_i = \frac{1 + \partial v_i/\partial x + v_i/(R+x)}{h_i}, \quad \text{and} \tag{16}$$

$$B_i = p_i + \frac{1}{2} v_i^2. \tag{17}$$

b. Restriction to a vertical section normal to the coast

Equation (15), which relates the alongshore and time dependency of the problem, will be neglected until section 6. We restrict our attention to a single vertical section normal to the coastline (Fig. 2), in which the current structure is governed by (14), (16), and suitable boundary conditions. Within this section, the layer interface outcrops either on the surface or the bed at $x = b$. We index the upper layer by a streamfunction $\psi_1(x)$ where

$$\frac{\partial \psi_1}{\partial x} = v_1 h_1 \tag{18}$$

and $\psi_1 = 0$ at the inshore edge of the layer, which may be at the coast ($x = 0$) or at a surface outcrop ($x = b$). The total upper-layer transport through the section is $Q = \lim_{x\to\infty} \psi_1(x)$. Since potential vorticity is conserved

along streamlines we can write Π_1 as a function $\Pi_1(\psi_1)$, which does not change from one such section to another.

Note that, if the current structures within two sections (through two distinct coastal locations) have identical transport Q and potential vorticity structure $\Pi_1(\psi_1)$, they must also have the same Bernoulli function $B_1(\psi_1)$, since, by (14) and (16)–(18),

$$\frac{\partial B_1}{\partial \psi_1} = \frac{\partial B_1}{\partial x} \frac{\partial x}{\partial \psi_1} = \frac{1 + \partial v_1/\partial x + v_1/(R+x)}{h_1}$$

$$= \Pi_1(\psi_1) \tag{19}$$

and the oceanic value $B_1(Q)$ is assumed fixed. Thus, when we estimate the adjustment in structure of a jet as it encounters gradually changing topography, we can make calculations based purely on conservation of potential vorticity and Q. Bernoulli function conservation is assured even though we do not explicitly consider the dynamics of the adjustment between one section and another.

The problem is greatly simplified if potential vorticity is assumed to be constant in each layer, since this precludes vorticity wave perturbations to the calculated steady states. The possibility of criticalities to these wave types is removed, eliminating the additional conjugate structures that such criticalities would support (Hughes 1985b; Woods 1988). The only remaining coastal-trapped wave modes are internal Kelvin-like since all barotropic modes are removed by the rigid-lid assumption. Following GS79, the lower layer is assumed to be of deep ocean origin with zero potential vorticity and the upper layer has potential vorticity everywhere equal to its value far offshore where velocities are negligible:

$$\Pi_1(\psi_1) = \Pi_1(Q) = 1, \tag{20a}$$

$$\Pi_2(\psi_2) = 0. \tag{20b}$$

Offshore of the shelf edge (at $x = W$) the lower layer is assumed to be deep and motionless

$$v_2 = 0 \quad \text{for } x \geq W. \tag{21}$$

Over the shelf, (16) and (20b) imply that

$$\frac{\partial v_2}{\partial x} = -1 - \frac{v_2}{R + x}, \tag{22}$$

which can be solved for $v_2(x)$ subject to (21) with no dependence on the upper-layer solution. Similarly, for the upper layer,

$$\frac{\partial v_1}{\partial x} = h_1 - 1 - \frac{v_1}{R + x} \tag{23}$$

and the momentum equation (14) is

$$\frac{\partial p_1}{\partial x} = \frac{v_1^2}{R + x} + v_1. \tag{24}$$

Subtracting (14) for the lower layer gives

$$\frac{\partial h_1}{\partial x} = \frac{v_1^2 - v_2^2}{R + x} + v_1 - v_2. \tag{25}$$

Far offshore ($x \rightarrow \infty$, $v_2 = 0$), (23) and (25) are satisfied by $v_1 = Ce^{-x} + De^x$, where C and D are constants. In order that v_1 does not grow offshore we require that $D = 0$, so

$$\frac{\partial v_1}{\partial x} + v_1 \rightarrow 0 \quad \text{as } x \rightarrow \infty. \tag{26}$$

Also,

$$p_1 = h_1 \rightarrow 1 \quad \text{as } x \rightarrow \infty. \tag{27}$$

Boundary conditions at a surface interface outcrop are

$$\psi_1 = h_1 = 0 \quad \text{at } x = b \quad \text{and} \tag{28}$$

$$v_1 = v_0 \quad \text{at } x = b, \tag{29}$$

where v_0 is a constant to be determined, defined as $v_1(x)$ at the inshore edge of the upper layer. When the interface outcrops on the bed

$$\psi_1 = 0 \quad \text{at } x = 0, \tag{30}$$

$$v_1 = v_0 \quad \text{at } x = 0, \quad \text{and} \tag{31}$$

$$h_1 = H \quad \text{for } x \leq b, \tag{32}$$

where $H(x)$ is the depth of the bed.

A useful result is that, using (14), (16), and (17), total upper-layer transport

$$Q = \int_0^\infty v_1 h_1 \, dx = \int_0^\infty v_1 \left(1 + \frac{\partial v_1}{\partial x} + \frac{v_1}{R + x}\right) dx$$

$$= \int_0^\infty \frac{\partial B_1}{\partial x} \, dx = B_1(\infty) - B_1(0) \tag{33}$$

when the upper layer extends to the coast, or $Q = B_1(\infty) - B_1(b)$ when the inshore edge of the upper layer is a surface outcrop at $x = b$. Since $p_1(\infty) = 1$ and $v_1(\infty) = 0$,

$$Q = 1 - p_0 - \frac{1}{2}v_0^2, \tag{34}$$

where p_0 is the value of $p_1(x)$ at the inshore edge of the upper layer.

3. Flow past a cape with no coastline curvature

When the coastline is straight ($R \rightarrow \infty$) and the topography slopes uniformly toward the ocean, (21)–(32) can be solved analytically (GS79). Solutions presented here differ from those of GS79 in that the depth of the shelf edge is fixed, with the result that the shelf steepens as it narrows, whereas GS79 fixed the shelf gradient allowing the depth of the shelf edge to vary. Both of these approaches are drastic approximations to realistic topography, but the shelf that steepens around a cape appears to better represent capes such as Cape Blanco on the Oregon coast (section 5). Thus, topography is given by

$$H(x) = \begin{cases} H_0 x/W & \text{if } x \leq W \\ \infty & \text{if } x > W, \end{cases} \tag{35}$$

where H_0 is the depth of the shelf edge and W is the shelf width. The inshore edge of the interface is at $x = b$, but in order to differentiate between surface and bed outcrops, a parameter α is introduced, defined as

$$\alpha = \begin{cases} b & \text{outcrop on surface} \\ -b & \text{outcrop on bed} \\ -W\Delta/H_0 & \text{outcrop below the shelf edge,} \end{cases} \tag{36}$$

where $\Delta = h_1(W)$.

The analytic approach is straightforward, following GS79, so details are omitted here, although solutions $v_1(x)$, $v_2(x)$, $h(x)$, and $p_1(x)$, as well as values of Q and the phase speed c of Kelvin-like perturbations, are included in appendix A.

Consider a steady current flowing along a coast with topography satisfying (35) but with varying shelf width $W(y)$. It is instructive to consider Q as a function of the interface outcrop position α and the shelf width W (Fig. 3a). Alongshore changes in the current structure must follow a Q contour (since Q is conserved), revealing how the position of the outcrop moves in response to changes in shelf width (Fig. 3b). For many values of the transport Q there are two possible current structures (with differing α) for a given shelf width W. These are conjugate structures. Any two conjugate structures are connected by a contour of Q that reaches a shelf width minimum W_{min} for some α. If the shelf were to narrow to exactly W_{min} and then widen again, a current flowing along this section of coast could distort smoothly from

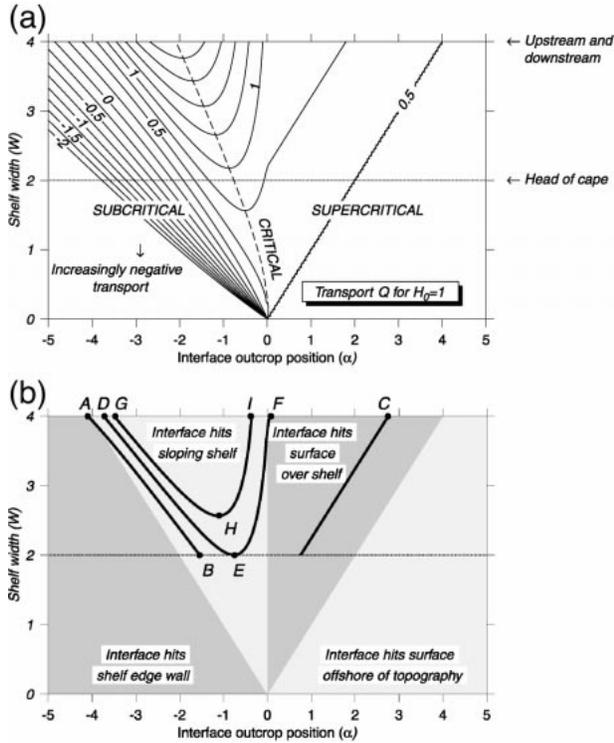FIG. 3. (a) Contoured transport Q for varying shelf width W and position of interface outcrop α. Shelf edge depth $H_0 = 1$. (b) Interpretive diagram for (a) showing four regimes of interface outcrop position. Three contours are shown: $Q = 0.6$ (AB and disjoint section to C), $Q = 0.922$ (DEF), and $Q = 1.2$ (GHI).

one structure to its conjugate by evolving through the sequence of solutions represented by the contour of Q. For a steady current it would be fortuitous for this *exact* circumstance to arise, but the time variation of a coastal upwelling jet takes it through a continuum of states. The evolving upwelling system will be represented crudely by assuming that the upstream α increases monotonically (though not necessarily linearly) with time. In other words, as the upwelling season develops, the interface moves up the bed toward the coast until it outcrops on the surface, then moves offshore (e.g., Allen 1980). The implicit assumption here is that the potential vorticity of the the upstream state is invariant in time. For now it will be assumed that the time evolution is sufficiently gradual that the system can be represented as a sequence of (increasingly upwelled) steady-state solutions.

As an example we consider a shelf that has a width $W = 4$, but narrows to $W = 2$ around a cape. This configuration is entirely equivalent to a narrowing of the shelf due to a canyon since the shape of the coastline is not important. The depth of the shelf edge is equal to the depth of the interface far offshore (i.e., $H_0 = 1$) and the alongshore scale of the cape is long so curvature is insignificant. Figure 3b highlights three contours of Q for $W \in [2, 4]$, corresponding to three regimes of behavior. The contour corresponding to the lower transport $Q = 0.6$ is split into two disjoint segments (A to B and the segment to C). Thus, although conjugate solutions exist there is no way of smoothly moving between them when W lies in this range. A current with this transport would distort as it rounded the cape (Figs. 4a and 5a) by following the Q contour from A to B, but would have to retrace the same sequence of solutions as the shelf widened again, returning to A and never reaching C. This solution is everywhere subcritical.
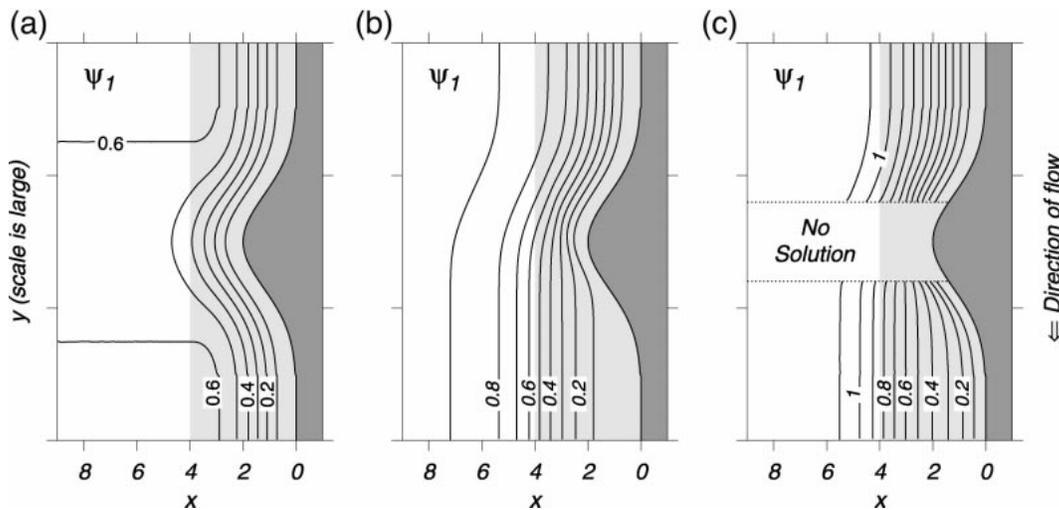

FIG. 4. Streamfunction for flows of varying transport Q as they pass a narrowing of the shelf from 4 to 2 Rossby radii. Coastline curvature is neglected and the y scale is assumed large. Transports are (a) $Q = 0.6$ (subcritical at head of cape), (b) $Q = 0.922$ (critical at head of cape), and (c) $Q = 1.2$ (no solution at the head of the cape). Pale shading shows the extent of the sloping shelf; $H_0 = 1$.
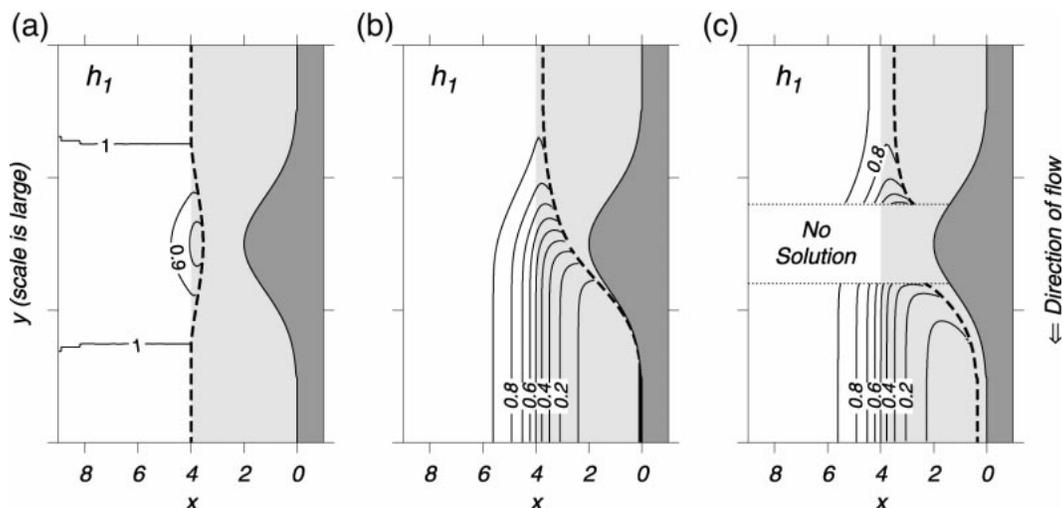
FIG. 5. As in Fig. 4 but showing interface depth h_1. A dashed bold line shows a bed outcrop and a solid bold line shows a surface outcrop (near the coast downstream of the cape in the critical case).

In contrast, $Q = 0.922$ is exactly critical when $W = 2$, so such a current would smoothly pass onto the conjugate branch of solutions (D to F via E in Fig. 3b) with a pronounced rise of the interface toward the surface in the lee of the cape (Fig. 5b) and a broadening of the current (Fig. 4b). The transition is from a subcritical state to a supercritical state via criticality. Sections through the jet (Fig. 6) show how dramatically the lower
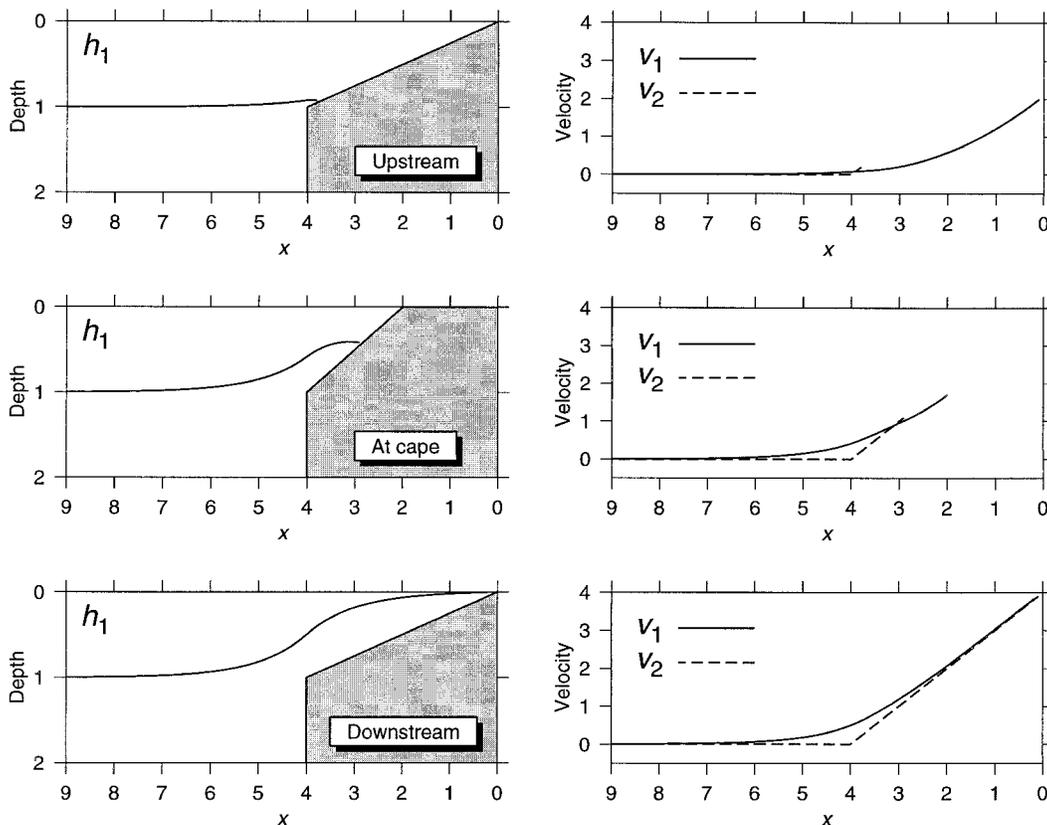

FIG. 6. Sections through the critical solution of Figs. (4) and (5) showing the interface shape (left column) and velocity structure (right column) at three locations: upstream (top), at the head of the cape (center), and downstream (bottom); $Q = 0.922$, $H_0 = 1$.
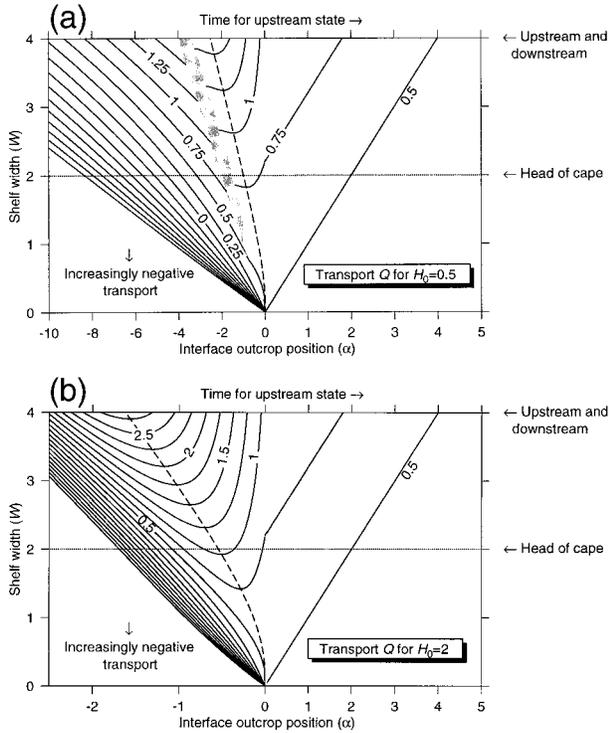
FIG. 7. Contoured transport Q for varying shelf width W and position of interface outcrop α with (a) $H_0 = 0.5$, (b) $H_0 = 2$. In the shaded region there are no valid solutions. The dashed lines indicate internal Kelvin wave criticality. Note, there is a scale change at $\alpha = 0$ such that the range of interface outcrop *depth* considered is the same in all cases.

layer pushes up onto the shelf. Velocities in both layers increase toward the coast, a consequence of having uniform potential vorticity that does not appear especially realistic. In the coastal ocean, the effect of friction would reduce velocities in this region.

When the transport is still higher, $Q = 1.2$, solutions only exist when the width is greater than some W_{min}. The current would distort from G to H (Fig. 3b), but when $W < W_{min}$ there is no solution that satisfies the hydraulic-scale assumptions and $\partial/\partial t = 0$, so the current must have significant alongshore gradients or time dependence. In hydraulically controlled systems, such a region is the source of nonlinear signals that propagate upstream and downstream, modifying the upstream and downstream conditions to reestablish a smooth critical transition. Such adjustments are considered in section 6. In Figs. 4c and 5c conjugate solutions are shown downstream once the shelf has widened sufficiently to permit solutions, but no claim is made that the flow would reestablish such a state.

It may seem contrived to set the shelf edge depth equal to the interface depth far offshore (i.e., $H_0 = 1$), but equivalent solutions with $H_0 = 0.5$ and $H_0 = 2$ (Fig. 7) show qualitative similarity. Compared with the $H_0 = 1$ solutions, the critical transport is higher ($Q = 1.046$ vs $Q = 0.922$) when $H_0 = 2$ (the shelf edge is twice
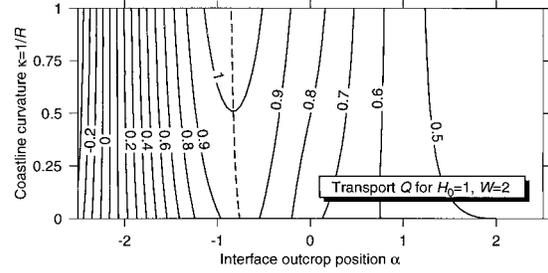

FIG. 8. Contoured transport Q for varying coastline curvature κ and position of interface outcrop α. Shelf width $W = 2$ corresponds to the head of the cape in the $\kappa = 0$ solutions. The dashed line indicates internal Kelvin wave criticality, which is here inferred from $\partial Q/\partial \alpha = 0$.

as deep as the interface far offshore) and lower ($Q = 0.799$) when $H_0 = 0.5$. Note that, when $H_0 = 0.5$, there is no valid solution within the shaded region of Fig. 7a. Analytic solutions can still be obtained, but the slope of the interface at its bed outcrop exceeds that of the bed itself.

4. Modification of the critical solution by curvature

Regions, such as capes, that permit a smooth transition in criticality often have significant curvature of the coastline and bathymetry. The effect of curvature in these regions is of particular interest since, by modifying the conditions required for criticality, the curvature may influence flow upstream and downstream of the critical region.

Consider a current flowing along a curved coastline. We adopt the convention that curvature $\kappa = 1/R$ is positive for a convexly curved coastline. Problems arise with negative curvature since $(R + x)$ is zero a finite distance offshore, leading to singularities of (22) to (25). These concavely curved solutions cannot be applied to coastal flows in which the current extends indefinitely offshore.

In the hydraulic approximation we must assume that κ varies only gradually alongshore so that we can locally take it to be constant. This requires that the amplitude of κ is small too, since otherwise the coastline would wrap around on itself. An attempt to represent a realistic coastline and topography by a sequence of solutions, in which κ and W vary alongshore, will be discussed in the next section.

When curvature terms are included (R is finite) the problem defined by (21)–(32) must be solved numerically. This is accomplished using a fourth-order integration scheme (appendix B), with a root-finding procedure to find solutions that satisfy the boundary conditions. Taking the solution of the previous section ($\kappa = 0$, $H_0 = 1$) at the head of the cape ($W = 2$) we consider the effect of varying κ in the range $\kappa \in [0, 1]$. Figure 8 shows contours of Q for varying κ and interface
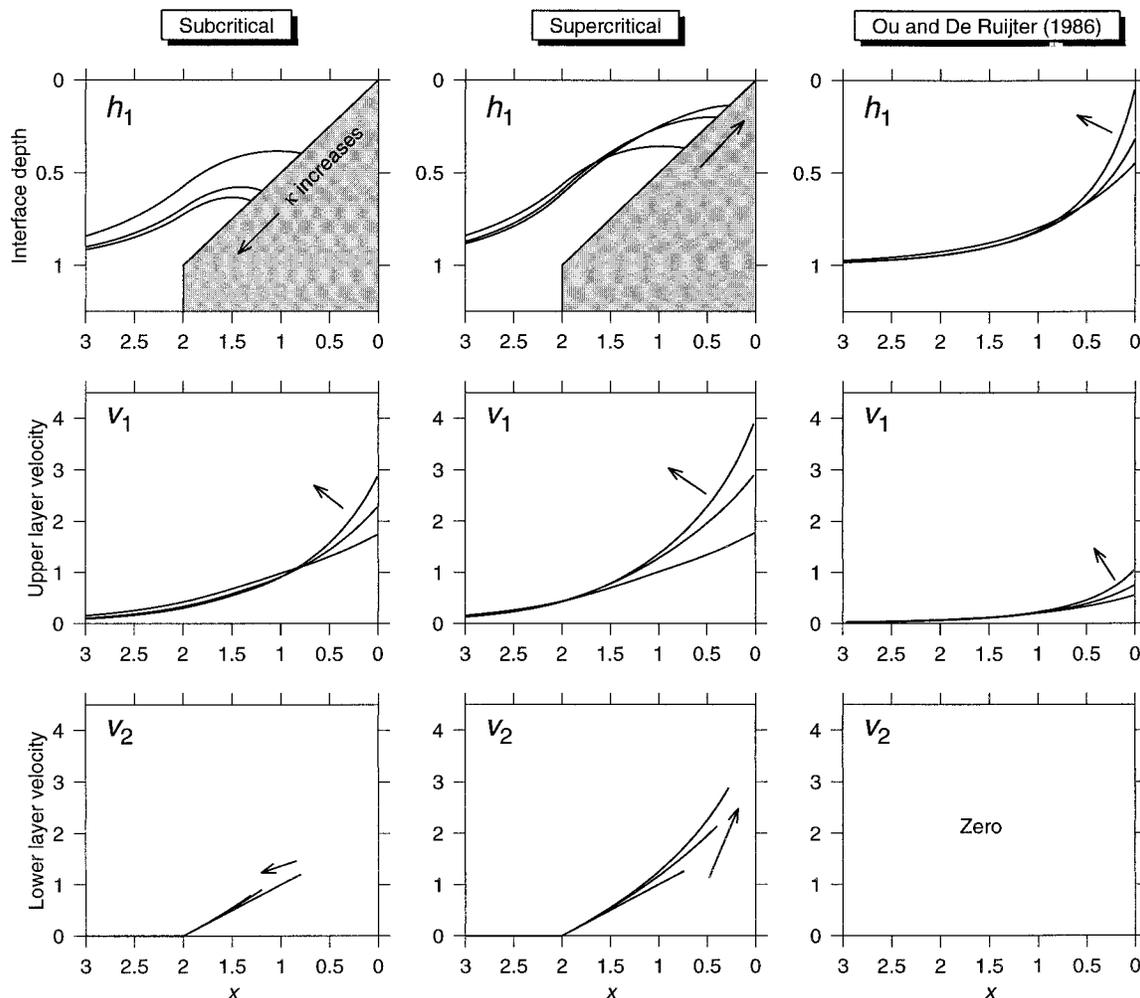
FIG. 9. The effect of varying coastline curvature $\kappa = 0, 0.5, 1$ on the solution at the head of the cape ($W = 2$) when transport Q is fixed at $Q = 0.92$, $H_0 = 1$. This Q is slightly less than the maximum (critical) transport for this W, so it permits both subcritical (first column) and supercritical (second column) solutions. The third column shows a solution with $Q = 0.4$ and no topography (following Ou and De Ruijter 1986). Arrows show the sequence of solutions for increasing κ.

outcrop position α. These contours would be the evolution paths (as they were in Fig. 3) of a steady current flowing along a coastline with varying $\kappa(y)$ and fixed $W(y)$, but in the present context both κ and W vary alongshore, so Fig. 8 should only be interpreted as a representation of the possible solutions at the head of the cape.

It is evident from Fig. 8 that the critical transport Q (corresponding to the dashed line in the figure) actually increases with κ. Thus, the more curved the head of the cape is, the greater transport is needed before a critical transition can take place to a strongly upwelled downstream state. This result is opposite to that of Ou and De Ruijter (1986), who found that a convex (positive) curvature encourages the interface to rise toward the surface and the current to eventually separate from the coast. The crucial difference of the present case is the inclusion of lower-layer dynamics and interaction with

topography. The response of a current structure to curvature is found to depend on its criticality (Fig. 9). In all cases (subcritical, supercritical, and Ou and De Ruijter's) the current at the coast intensifies and becomes increasingly sheared as curvature increases. The difference lies in the effect on the interface outcrop. Increasing curvature causes the outcrop of a supercritical solution to move up the bed toward the coast, whereas the outcrop of a subcritical solution moves farther down the bed, opposing a critical transition.

5. An approximation to Cape Blanco

We now consider a realistic cape (Cape Blanco), approximated in such a manner that flow fields can be constructed from solutions of the type considered in the preceding two sections. Such an approach allows us to estimate the validity of the hydraulic assumptions when
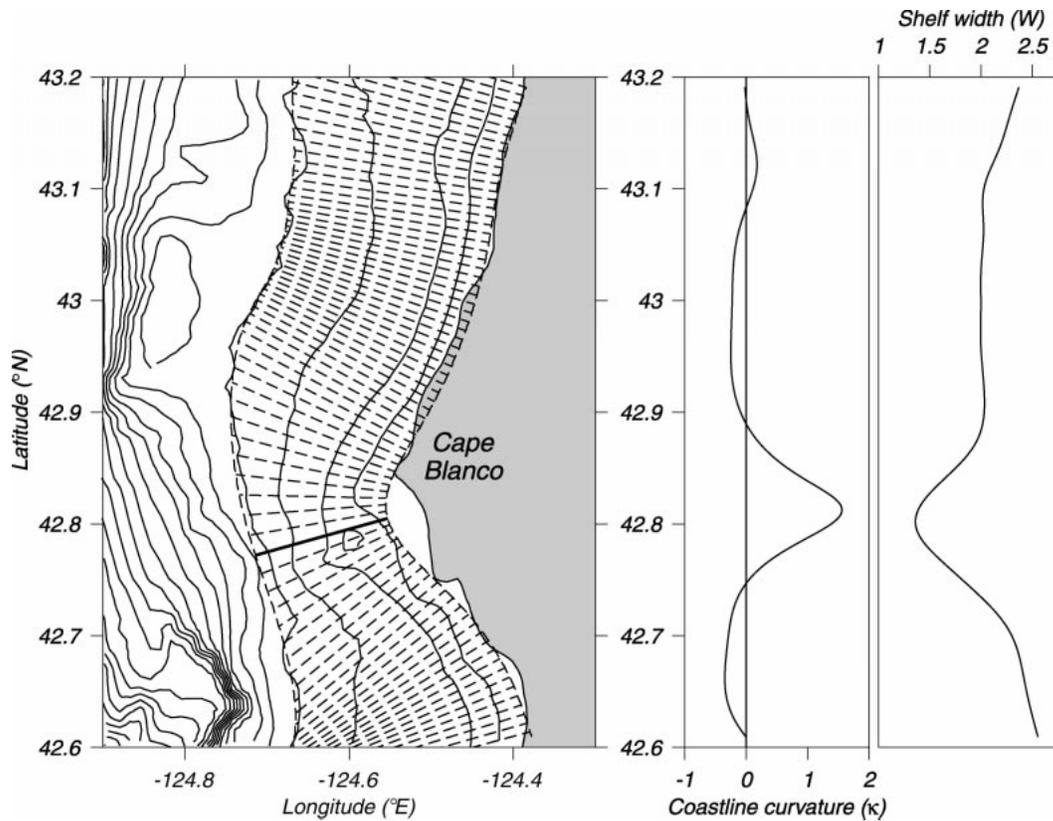
FIG. 10. Topography of the region around Cape Blanco, Oregon, with the linear shelf approximation used in the text. Dashed lines represent the approximated coast and shelf edge. Lines normal to the coast along which solutions are computed are also shown. The line with the lowest critical transport is highlighted. Isobaths are at 20 m and multiples of 50 m. Panels show nondimensional W and κ with lengthscale $a = 10$ km, the internal Rossby radius.

the topography varies with realistic alongshore lengthscales. We can also add realistic scalings to the results of the previous sections, and so determine whether criticality is likely to occur for observed upwelling jet transports.

Density observations from offshore of the upwelling jet close to Cape Blanco at the time of the SST image (Fig. 1) give a first Rossby radius of deformation of close to 10 km. This is used as the horizontal lengthscale (a). The offshore interface depth (h_∞) is estimated from the position of the main pycnocline to be 100 m. An f plane is assumed, with $f \approx 1 \times 10^{-4}$ in this region, so a scale for the transport Q is $a^2 h_\infty f = 1$ Sv (Sv $\equiv 10^6$ m^3 s^{-1}). We wish to approximate the topography by a linearly sloping shelf. The shelf edge is well represented by the 150-m isobath (so $H_0 = 1.5$), but using the actual coastline may lead to an underestimate of the effective shelf gradient because in places (and particularly immediately to the southwest of Cape Blanco) shoals extend a significant distance offshore. We avoid this problem by determining the shelf gradient between (smoothed) 20-m and 150-m isobaths, then extrapolating inshore to zero depth for an estimate of coastline position. This procedure pulls our estimated coastline offshore in the lee of the cape (Fig. 10). Note that the

bank offshore of our approximated shelf edge (at 43°N), which rises to within 100 m of the surface, and Heceta bank (44.25°N), to the north of our region of interest, have been ignored, although these features undoubtedly have a strong influence on the flow in this region.

For the topography of Fig. 10, jet transport is calculated (Fig. 11) in sections normal to the coast as a function of the coastal latitude of each section and interface outcrop position α. In these calculations, negative κ has been neglected, but positive κ has been taken into account. Critical transport $Q = 0.757$ corresponds to a contour of Q that can smoothly pass from a subcritical upstream solution (A in Fig. 11), through exact criticality (B), to a supercritical downstream solution (C). Exact criticality occurs slightly to the south of the cape, close to where the shelf width is a minimum. A two-dimensional flow field at the critical transport is constructed by linking the one-dimensional solutions from a series of points along the coast. In particular, two-dimensional fields of ψ_1, p_1, and h_1 can be determined. Flow normal to the coast and bathymetry is implied by the two-dimensional streamfunction, since such flow is required in order to make alongshore adjustments. Note, however, that this component of velocity has still been neglected in calculating the one-dimen-
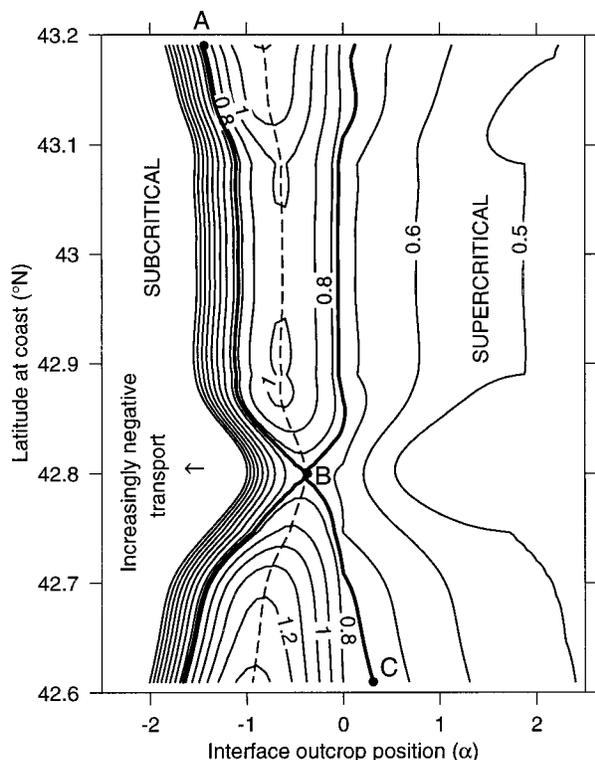
FIG. 11. Transport Q as a function of interface outcrop position α and latitude at the coast for the approximated Cape Blanco topography. Critical solutions lie on the dashed line. The bold contour $Q = 0.757$ corresponds to the lowest critical transport. At this Q a current may smoothly transition from a subcritical upstream state A through a critical state B to a supercritical downstream state C.

sional solutions. This means that our two-dimensional flow field cannot satisfy the steady ($\partial/\partial t = 0$) momentum equation exactly. We estimate the extent of the discrepancy by calculating

$$\epsilon = \frac{|\mathbf{u}_1 \cdot \nabla \mathbf{u}_1 + \nabla \psi_1 + \nabla p_1|}{|\nabla p_1|}, \qquad (37)$$

where $\mathbf{u}_1 = (u_1, v_1)$ and ∇ is the horizontal gradient operator. Here ϵ is the error in the upper-layer momentum equation [a nondimensional (1) and (2) expressed in vector form, with $\partial/\partial t = 0$] normalized by the (usually) dominant pressure gradient term. An acceptable steady solution would have $\epsilon \ll 1$.

The flow field (Fig. 12) is superficially similar to the critical solution of section 3 (Figs. 4 and 5). Values of ϵ are greater than 0.1 over 57% of the domain of the figure. Upstream of the cape, bands of large ϵ occur normal to the coast where rapid changes in W or κ (the parameters of the one-dimensional problem) require alongshore adjustment of the solution, although, to some extent, the suddenness of these adjustments can be attributed to the method by which the two-dimensional solution has been constructed. Here ϵ remains relatively small around the head of the cape approaching the critical section. As the flow becomes supercritical, ϵ is large close to the interface outcrop on the bed (around 42.75°N) where rapid adjustments are taking place. Farther downstream, the velocities and accelerations in the (now shallow) upper layer are large, again leading to elevated values of ϵ.

Neglecting curvature effects (Fig. 13) removes the adjustment required for alongshore variations in κ, but leads to elevated ϵ around the head of the cape where
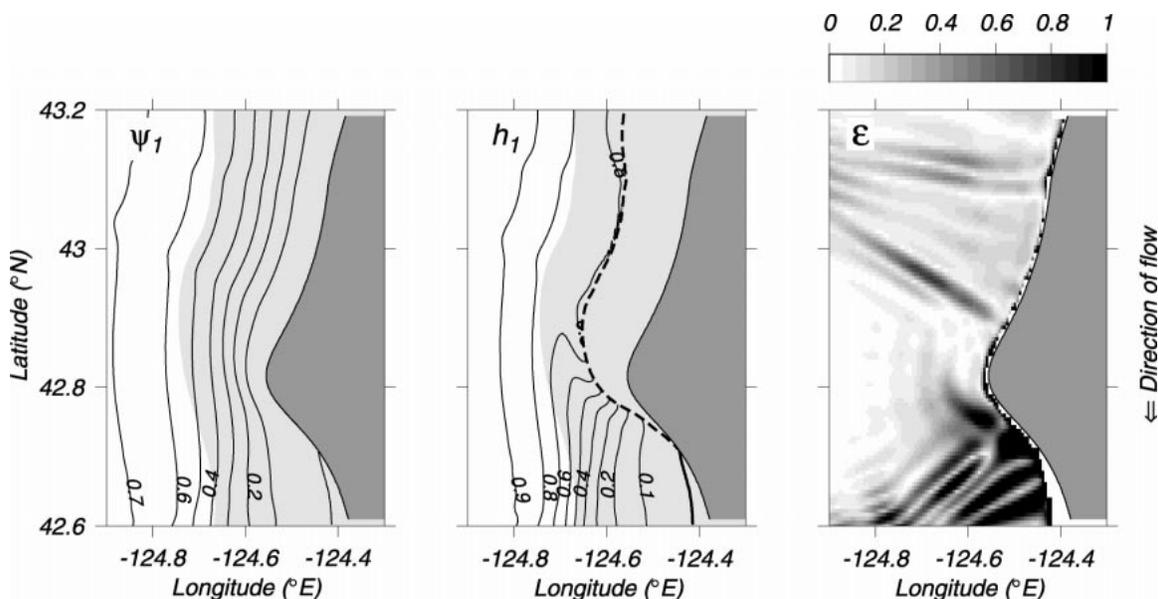

FIG. 12. Fields of (left to right) streamfunction ψ_1, interface depth h_1, and error of the two-dimensional solution ϵ for approximated Cape Blanco topography and critical transport; $Q = 0.757$. Pale shading shows the extent of the sloping shelf. A dashed bold line shows a bed outcrop and a solid bold line shows a surface outcrop.
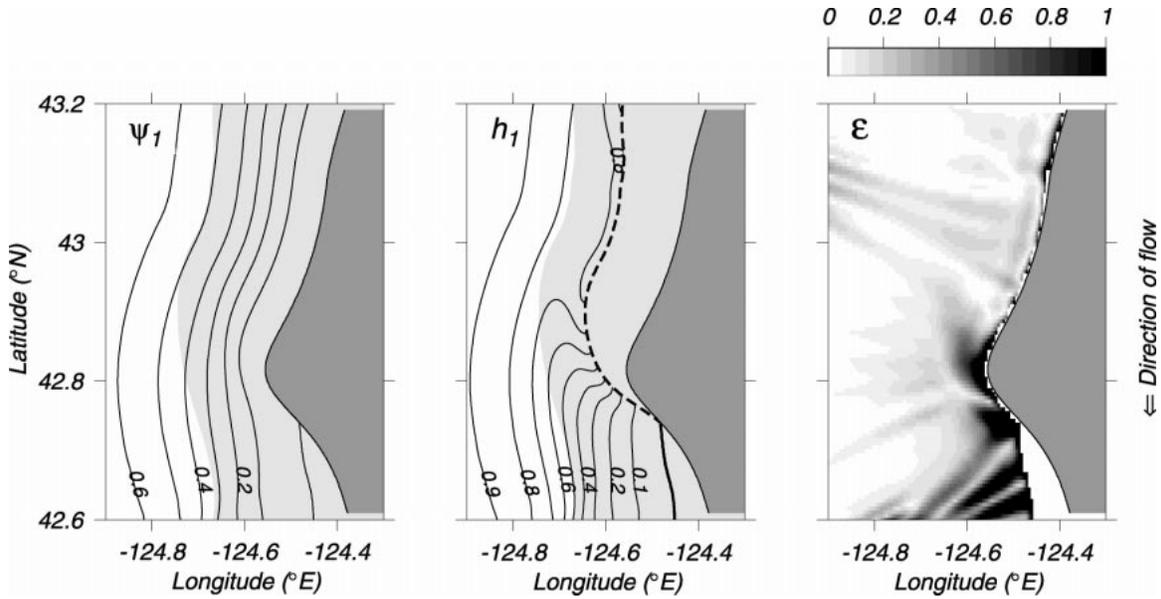
FIG. 13. As in Fig. 12 but with curvature of the coastline and flow field neglected. The critical transport is reduced to $Q = 0.710$.

the pressure field is no longer providing an onshore acceleration to take the current around the bend in the coastline. The critical transport reduces to $Q = 0.710$, as expected from the results of the previous section.

It is clear from the elevated values of ϵ that Cape Blanco is a rather abrupt feature as far as hydraulic theory is concerned. At critical transports, alongshore adjustments in cross-shore structure could never be rapid enough to match the changes in the topography and the direction of the coastline. The current would meander as it attempted to adjust in the lee of the cape. While linear disturbances to the essentially supercritical flow would be swept downstream, this would not necessarily be true of nonlinear disturbances. In addition, such disturbances could gain energy through baroclinic instability (Mitsudera and Grimshaw 1994).

6. Time-dependent solutions

We now consider the evolution in time of the steady solutions considered so far. The alongshore and time dependence of solutions are related by (15). In the limit $R \rightarrow \infty$, (14) and (15) are semigeostrophic since only the cross-shore momentum balance is geostrophic. This is a consequence of the scaling assumptions of section 2, and here is equivalent to a long-wave approximation. In a cross-shore slice the problem is exactly that considered in section 3, so we can make use of the analytic solutions of appendix A.

Consider a straight coastline bordering a shelf of varying width $W(y)$. Since u is zero at the coast, (15) implies that

$$\left[\frac{\partial v}{\partial t} + v \frac{\partial v}{\partial y} + \frac{\partial p}{\partial y} \right]_{x=0} = 0. \qquad (38)$$

When the interface outcrops on the sloping shelf [case (c) of appendix A], the coastal velocity $v_0(y, b(y, t), W(y))$ and pressure $p_0(y, b(y, t), W(y))$ satisfy

$$\frac{\partial v_0}{\partial t} + v_0 \frac{\partial v_0}{\partial y} + \frac{\partial p_0}{\partial y} = 0, \qquad (39)$$

(again appealing to the straightness of the coastline). So, in view of (34),

$$\frac{\partial v_0}{\partial t} = \frac{\partial Q}{\partial y} \qquad (40)$$

and a solution in which Q is constant alongshore (as in section 3) is a steady state. Applying the chain rule to (39), and substituting the more general $\alpha(y, t)$ [defined by (36)] for $b(y, t)$ gives an equation relating the derivatives of $\alpha(y, t)$ to variations in W:

$$\frac{\partial \alpha}{\partial t} \frac{\partial v_0}{\partial b} = -\frac{\partial \alpha}{\partial y} \left[v_0 \frac{\partial v_0}{\partial b} + \frac{\partial p_0}{\partial b} \right] + \frac{\partial W}{\partial y} \left[v_0 \frac{\partial v_0}{\partial W} + \frac{\partial p_0}{\partial W} \right]. \quad (41)$$

Coefficients involve the known expressions (A20) and (A21) for v_0 and p_0. Equation (41) can be solved for $\alpha(y, t)$ as an initial value problem by integrating in time from a known state $\alpha(y, 0)$. This is numerically straightforward, although nonlinearity leads to wave steepening, which must be controlled by adding a diffusive term $A_y \partial^2 \alpha / \partial y^2$ to $\partial \alpha / \partial t$ in order to prevent numerical instability. With this modification, solutions can support propagating bores, but it must be emphasized that the dynamics of these bores is not represented by the semigeostrophic equations since they violate the scaling assumptions of section 2. Their propagation speed is largely determined by the value of A_y, which in turn is chosen purely on the grounds of numerical stability

(here, $A_y = 5 \times 10^{-3}$, $\Delta y = 5 \times 10^{-3}$ and $\Delta t = 1 \times 10^{-4}$).

When the interface lies on the vertical wall at the shelf edge [case (d) of appendix A], $\alpha(y, t)$ evolves according to

$$\frac{\partial \alpha}{\partial t} \frac{\partial v_0}{\partial \Delta} = \left(\frac{\alpha}{W} \frac{\partial W}{\partial y} - \frac{\partial \alpha}{\partial y} \right) \left[v_0 \frac{\partial v_0}{\partial \Delta} + \frac{\partial p_0}{\partial \Delta} \right]$$
$$+ \frac{W}{H_0} \frac{\partial W}{\partial y} \left[v_0 \frac{\partial v_0}{\partial W} + \frac{\partial p_0}{\partial W} \right] \quad (42)$$

with $\Delta(y, t)$ replacing $b(y, t)$ of (41) and extra terms arising from the fact that $\alpha = -W\Delta/H_0$, where W is a function of y. For completeness, the equivalent expression in case (a), when the interface outcrops on the surface offshore of the shelf edge, is

$$\frac{\partial \alpha}{\partial t} = 0, \quad (43)$$

and in case (b), when the outcrop is onshore of the shelf edge,

$$\frac{\partial \alpha}{\partial t} \left[\frac{\partial v_1}{\partial b} \right]_{x=b} = -\frac{\partial \alpha}{\partial y} \left[v_0 \frac{\partial v_0}{\partial b} + \frac{\partial p_0}{\partial b} \right]$$
$$- \frac{\partial W}{\partial y} \left[v_0 \frac{\partial v_0}{\partial W} + \frac{\partial p_0}{\partial W} \right], \quad (44)$$

although in the solution presented here the interface never surfaces.

We consider the situation of section 3, in which a shelf narrows from $W = 4$ to $W = 2$ around a cape. The narrowing of the cape has Gaussian alongshore form with an alongshore extent of order 1 (much larger than cross-shore scales since $L \gg a$). The purely subcritical state of Fig. 5 ($Q = 0.6$, $H_0 = 1$) is used as an initial condition $\alpha(y, 0)$, representing the situation early in the upwelling season. In view of (40) the initial state does not evolve unless forced or perturbed. Forcing is provided by adding a contribution $\partial \alpha / \partial t = 0.1$ during the period $0 \le t \le 10$. This crudely models steady upwelling since, as mentioned earlier, increasing α represents increasingly upwelled states. The response (Fig. 14) shows a jet that gradually increases in strength until, at around $t = 4.5$, it becomes critical at the head of the cape ($y = 5$) and transitions to its conjugate supercritical solution (thick curve in Fig. 14), which extends downstream with a bore at its leading edge. The bore marks the transition back to the subcritical conditions that still exist far upstream and downstream. As mentioned previously, the dynamics of this bore are not represented. Nevertheless, there is a pleasing resemblance to the SST image of Fig. 1, which shows the offshore extent of upwelled water broadening at Cape Blanco then suddenly reverting back to a narrower state around 42.1°N.

At $t = 10$ the forcing to α ceases and the solution is allowed to evolve to a steady state. By $t = 14$ the bore

has traveled out of the domain and the solution has settled down to $Q = 0.922$ everywhere, with exact criticality at the head of the cape (cf. Fig. 5b). At $t = 15$ the critical solution is perturbed by an impulsive upwelling event represented by suddenly increasing α everywhere by $\Delta \alpha = 0.5$. The system responds by producing transient waves that propagate up- and downstream, reestablishing the steady, critical solution. This is hydraulic control since the nature of the topography at the head of the cape is prescribing the upstream and downstream flow by establishing its own criticality.

7. Discussion

Despite the obvious simplicity of the GS79 model, the predicted flow field in the critical transition case looks very much like the phenomena observed in the lee of capes in upwelling regions (Fig. 1). In particular, the offshore movement of the jet (Fig. 4) and the strong upwelling in the lee of the cape (Fig. 5) are well represented. Although dense water does not outcrop downstream in the analytic solution as it does in the SST image (Fig. 1), it should be remembered that this is a two-layer approximation to a continuously stratified system. The combination of a less sharp density interface and surface mixing would bring dense water to the surface where the interface is shallow. When the topography approximates Cape Blanco (Fig. 10), the parameters of the problem are such that the lower layer does actually surface downstream of the cape.

Perhaps the least realistic aspect of GS79 is the assumption of constant potential vorticity in each layer. It was this assumption that permitted analytic progress by restricting the coastal-trapped waves supported by the system to internal Kelvin-like waves. Under the constant potential vorticity assumption the velocity in a layer becomes increasingly sheared as that layer thins toward its inshore edge, with the result that the maximum velocity occurs at this edge where the layer thickness approaches zero (Fig. 6). It would seem natural to choose a potential vorticity structure based on a motionless pre-upwelling state with a flat interface, but such a state would have arbitrarily large potential vorticity nearshore as the depth approached zero. A further problem is that potential vorticity is modified by frictional effects that are not permitted by our premise of potential vorticity conservation. It should be noted, however, that the concept of a critical transition of structure does not require potential vorticity to be conserved since criticality is only required in a single cross-shore section (here, the head of the cape). The criticality or otherwise of this section depends on the local potential vorticity structure, irrespective of whether this varies along streamlines.

No studies of coastal hydraulics have yet allowed changes in potential vorticity along streamlines. Nonuniform potential vorticity distributions that permit shear/vorticity type waves have been considered both
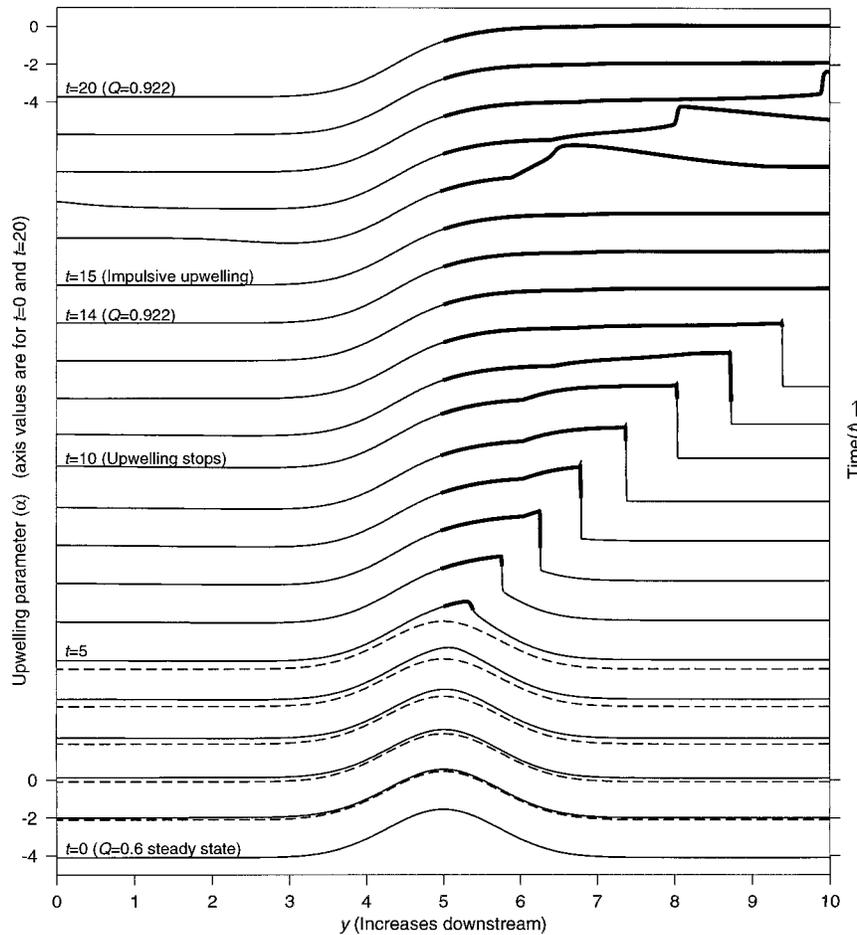
FIG. 14. Evolution from an initially steady, subcritical state ($Q = 0.6$) under the influence of continued upwelling. A Gaussian cape is centered at $y = 5$. Upstream and downstream, $W = 4$, narrowing to $W = 2$ at the cape; $H_0 = 1$. The interface outcrop position $\alpha(y, t)$ is shown at intervals $\Delta t = 1$, stacked vertically. The initial state is superimposed (dashed) as a reference in the early stages of the evolution. Upwelling is continuous during the period $0 \leq t \leq 10$ with additional impulsive upwelling at $t = 15$ (see text). The supercritical portion of solutions is shown by a thick curve.

in one layer with topography (Hughes 1985a,b) and in two layers without topography (Woods 1988). The next step toward realism would be to consider two layers with realistic potential vorticity distribution as well as bottom topography. Such a system is the subject of ongoing research. For a layer model of coastal hydraulics to be a good approximation to a continuously stratified system, its governing criticalities must be similar to those of the more complex system. This could be demonstrated by direct calculation of the phase speed of stable coastal-trapped wave modes of the continuous system. Luther and Bane (1985) have calculated unstable modes of such a system by a method that could also be used to find stable modes.

It seems intuitively obvious that convex coastline curvature should encourage a coastal jet to separate from the coast. However, care must be taken to distinguish between separation arising from an inability of the cur-

rent to adjust its structure to match a rapidly curving coastline ($\partial/\partial y$ becomes significant) and the hydraulic mechanism, based on potential vorticity conservation, in which it is always assumed that such adjustment can take place. In a baroclinic system with one active layer and no topography (Ou and De Ruijter 1986) or a barotropic system with topography (Hughes 1989), convex curvature does indeed encourage flow separation for purely hydraulic reasons. The case considered here is essentially similar to Ou and De Ruijter except for the addition of simple dynamics describing the interaction of the lower layer with topography. This modification reverses the effect of curvature since convex curvature now causes the interface of a subcritical solution to move down the bed away from the coast, opposing a critical transition to a strongly upwelled downstream state. The curvature-induced increase in the critical transport is small, around 8% for topography approxi-

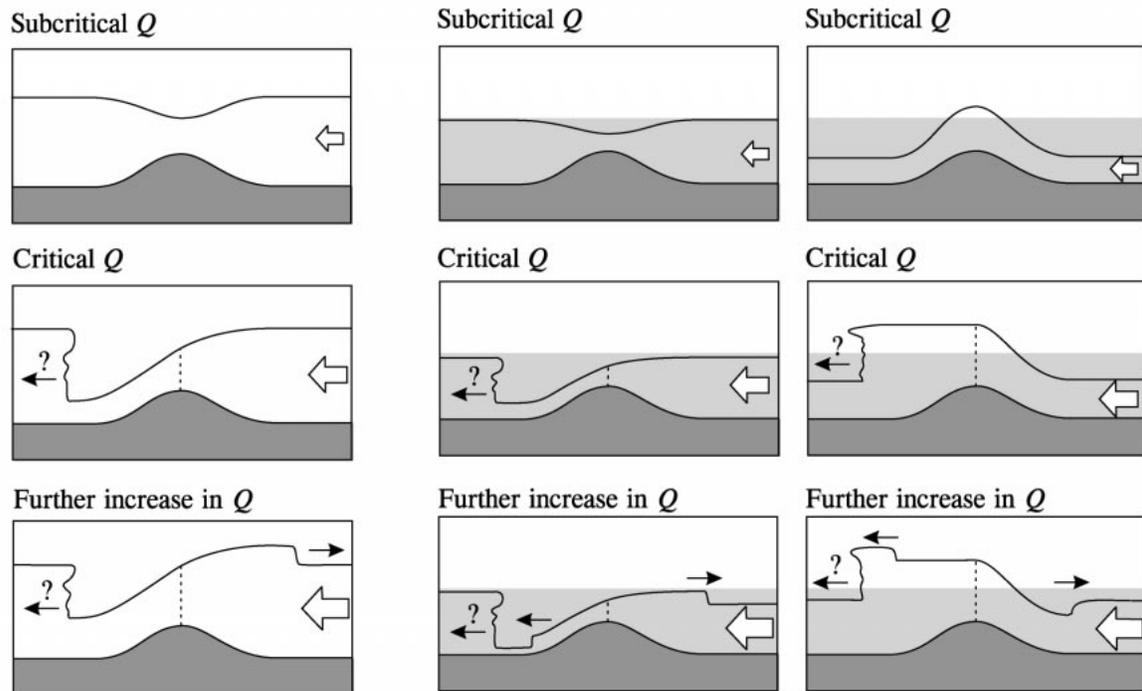**Channel hydraulics (Long,1972)**   **Coastal hydraulics**

FIG. 15. Hydraulically controlled channel flow over an obstacle (Long 1972) and its analog for coastal flow past a cape. The channel hydraulics are represented by a vertical section showing the fluid surface, whereas the coastal hydraulics are represented by a horizontal section showing the position of the interface outcrop on the bed (center column) and the effect on a line of particles initially released a uniform distance from the coast (right-hand column). Direction and magnitude of Q are shown by the white arrow. Pale shading shows the extent of the sloping shelf. A dashed line indicates a critical transition from subcritical upstream to supercritical downstream conditions. Further description in the text.

mating Cape Blanco, but the required adjustment in the cross-shore structure of the jet to accommodate curvature effects may be significant (producing a band of large ϵ normal to the shore in Fig. 12) and initiate meandering or separation for other reasons.

The estimated critical transport for Cape Blanco is 0.76×10^6 m^3 s^{-1} (Fig. 11), although much of this transport comes from the (probably spurious) shear in shallow water resulting from the constant potential vorticity assumption. It is encouraging, however, to note a close agreement with the measured transport of the jet off the Oregon coast. In August 1994 the estimated southward transport off Cape Blanco, based on geostrophic velocities referenced to no motion at 200 m, was 0.93×10^6 m^3 s^{-1} (Barth et al. 2000). A confident determination of the relevance of hydraulic theory to the flow around Cape Blanco will require calculations based on more realistic dynamics.

Perhaps the most interesting aspect of the hydraulics of upwelling jets is the time variation of the upstream conditions. On a simple level this can be seen as serving to find the critical solution since we have an evolution through a continuum of states and need not rely on chance criticality. But what happens when critical conditions are established at the cape and upwelling con-

tinues upstream? This is where the concept of hydraulic control becomes relevant and analogies can be drawn with other physical systems. Channel flow over an obstacle (Long 1972) has many parallels with the current problem (Fig. 15). Long's tank experiments used a channel containing water that was initially at rest with an obstacle on the bed. The obstacle was impulsively set in motion along the channel creating an initial transient response and a steady disturbance that moved with the obstacle. For flow that was subcritical everywhere (relative to the obstacle) the steady state was symmetric about the obstacle (cf. Figs. 4 and 5, left panels). Stronger flow that was critical over the obstacle made a smooth transition to supercriticality (cf. Figs. 4 and 5, center panels) with an adjustment to the subcritical downstream state via a hydraulic jump (stationary) or a propagating bore. Based on the results of section 6, the analogous situation for a coastal jet (Fig. 15, center right) has a structure that broadens as it undergoes critical transition at a cape, then suddenly narrows downstream as it jumps back to a subcritical state. This situation resembles that seen around Cape Blanco in May 1995 (Fig. 1).

In Long's channel experiment, when the flow speed was increased from an initially critical state, the obstacle

had a blocking effect. A bore was generated that propagated upstream, modifying the upstream state (both transport Q and Bernoulli function B) in such a manner that criticality was preserved over the obstacle. The method of imposing the flow increase (through towing the obstacle faster) led to alongshore variation of B. In our analogous coastal jet calculations (section 6), it has been assumed that the potential vorticity structure [and hence B, in view of (19)] does not vary with time, so an impulsive attempt to increase the flow (Fig. 14, $t = 15$) does not modify potential vorticity. The critical Q at the cape is thus fixed, and the response of already critical flow to further upwelling is a pair of nonlinear waves that propagate upstream and downstream, opposing upwelling and restoring this critical Q everywhere (Fig. 15, lower right). The nonlinear waves steepen to bores as they propagate, eventually violating the hydraulic scale assumptions. Wave steepening would be least rapid for small amplitude adjustments due to gradual attempts to increase Q through continued upwelling-favorable wind.

Off the Oregon coast upwelling-favorable winds do not blow consistently during the upwelling season but rather as a series of upwelling-favorable events separated by periods of weak or downwelling-favorable winds (Smith 1974). Following the spring transition to an upwelled state, subsequent periods of upwelling-favorable winds lead to no appreciable strengthening of the southward baroclinic jet observed well north of Cape Blanco near 45°N (Smith 1974; Huyer et al. 1979). The possibility that the system may be hydraulically controlled, as described above, is intriguing and worthy of further investigation.

8. Conclusions

It is encouraging that a simple hydraulic model, an extension of GS79, reproduces many of the observed features of the flow of an upwelling jet past a cape. In particular, the critical solution that makes a smooth transition in structure at a narrowing of the shelf shows an offshore movement of the jet and brings dense deep water close to the surface downstream. It has been established that the scales of the problem are relevant to Cape Blanco on the Oregon coast since the predicted critical transport is close to observed values (0.76 compared with 0.93×10^6 m^3 s^{-1}). However, the simple GS79 model does not necessarily represent well the most important coastal-trapped wave mode, so it remains to demonstrate near-criticality of a dynamically important mode of the coastal-trapped wave problem with realistic background current shear and continuous stratification.

The hydraulic assumption of long alongshore scales has been investigated for topography approximating Cape Blanco by predicting the inherent error in hydraulically calculated flow fields. The rapidity of adjustment through the critical section and downstream of the cape is not well represented, suggesting that actual flow would have greater alongshore and temporal variability than predicted. Further complexities at Cape Blanco include the poleward undercurrent and observed recirculation in the lee of the cape (Barth et al. 2000). In addition, the flow often has substantial alongshore variation in the form of eddies and squirts that carry water off the shelf (Barth and Smith 1998). So, it is not claimed here that typical upwelling flow around Cape Blanco is completely described by hydraulic theory, but certainly at times the flow pattern looks very much like hydraulic predictions.

Time-dependent, semigeostrophic calculations predict that, as an upwelling season progresses, the jet strengthens from a weak flow that is subcritical everywhere and symmetric about the cape, to a critical flow that transitions to a strongly upwelled, supercritical state downstream. This supercritical flow must at some point jump back to the subcritical conditions far downstream. The response to further upwelling demonstrates the implications of hydraulic control in coastal upwelling systems. The head of a cape becomes a control point, influencing the upstream and downstream flow. If the upstream potential vorticity structure does not change in time, the critical transport at the control point places an upper limit on the transport of the upwelling jet since after any further upwelling event the flow adjusts back to its critical state and transport.

APPENDIX A

Analytic Solutions for $R \to \infty$

For topography (35) and zero curvature, (21)–(32) can be solved analytically. The method closely follows GS79 so details are not given here.

The velocity in the lower layer (where it exists) is

$$v_2 = \begin{cases} W - x & \text{if } x \leq W \\ 0 & \text{if } x > W. \end{cases} \quad \text{(A1)}$$

The upper-layer solution is split into four cases based on where the interface outcrops on the surface or hits the topography.

Case (a): *Interface outcrops on the surface at $x = b \geq W$ (offshore of the shelf edge)*

For $x \geq b$

$$v_1(x) = e^{b-x} \quad \text{and} \quad \text{(A2)}$$

$$p_1(x) = h_1(x) = 1 - v_1(x): \quad \text{(A3)}$$

$Q = 0.5$ follows from (34). The phase speed of perturbations is

$$c = 0. \tag{A4}$$

Case (b): *Interface outcrops on the surface at $x = b \leq W$ (onshore of the shelf edge)*

For $x \geq W$

$$v_1(x) = \frac{1}{2}e^{W-x}(1 + e^{2(b-W)}) \quad \text{and} \tag{A5}$$

$$p_1(x) = h_1(x) = 1 - v_1(x). \tag{A6}$$

For $b \leq x \leq W$

$$v_1(x) = \frac{1}{2}e^{x-W}(1 + e^{2(b-x)}) + W - x, \tag{A7}$$

$$p_1(x) = \frac{1}{2}[e^{x-W}(1 - e^{2(b-x)}) - (x - W)^2], \quad \text{and} \tag{A8}$$

$$h_1(x) = \frac{1}{2}e^{x-W}(1 - e^{2(b-x)}). \tag{A9}$$

Then Q follows from (34)

$$Q = 1 - \frac{1}{2}e^{2(b-W)} + (b - W)e^{(b-W)}, \tag{A10}$$

and phase speed is

$$c = e^{b-W} - 1 - b + W. \tag{A11}$$

Case (c): *Interface hits the bed at $x = b \leq W$ (onshore of the shelf edge)*

For $x \geq W$

$$v_1(x) = \frac{1}{2}e^{W-x}(1 + e^{2(b-W)}) - \frac{H_0 b}{W}e^{b-x} \quad \text{and} \tag{A12}$$

$$p_1(x) = h_1(x) = 1 - v_1(x). \tag{A13}$$

For $b \leq x \leq W$

$$v_1(x) = \frac{1}{2}e^{x-W}(1 + e^{2(b-x)}) - \frac{H_0 b}{W}e^{b-x} + W - x, \tag{A14}$$

$$h_1(x) = \frac{1}{2}e^{x-W}(1 - e^{2(b-x)}) + \frac{H_0 b}{W}e^{b-x}, \quad \text{and} \tag{A15}$$

$$p_1(x) = h_1(x) - \frac{1}{2}(x - W)^2. \tag{A16}$$

For $x \leq b$

$$v_1(x) = v_0 + \frac{H_0 x^2}{2W} - x, \tag{A17}$$

$$p_1(x) = p_0 + v_0 x + \frac{H_0 x^3}{6W} - \frac{x^2}{2}, \quad \text{and} \tag{A18}$$

$$h_1(x) = H(x) = \frac{H_0 x}{W}, \tag{A19}$$

where

$$v_0 = v_1(0) = e^{b-W} - \frac{H_0 b}{W}\left(1 + \frac{b}{2}\right) + W \quad \text{and} \tag{A20}$$

$$p_0 = p_1(0) = -\frac{W^2}{2} - be^{b-W}$$

$$+ \frac{H_0 b}{W}\left(1 + b + \frac{b^2}{3}\right): \tag{A21}$$

Q follows from (34) and phase speed is

$$c = v_0 - 1 - b. \tag{A22}$$

Case (d): *Interface hits the vertical shelf edge at a depth $\Delta = h_1(W)$*

For $x \geq W$

$$v_1(x) = (1 - \Delta)e^{W-x} \quad \text{and} \tag{A23}$$

$$p_1(x) = h_1(x) = 1 - (1 - \Delta)e^{W-x}. \tag{A24}$$

For $x \leq W$

$$v_1(x) = v_0 + \frac{H_0 x^2}{2W} - x, \tag{A25}$$

$$p_1(x) = p_0 + v_0 x + \frac{H_0 x^3}{6W} - \frac{x^2}{2}, \quad \text{and} \tag{A26}$$

$$h_1(x) = H(x) = \frac{H_0 x}{W}, \tag{A27}$$

where

$$v_0 = v_1(0) = 1 - \Delta + W\left(1 - \frac{H_0}{2}\right) \quad \text{and} \tag{A28}$$

$$p_0 = p_1(0) = \Delta + W(\Delta - 1) + \frac{W^2}{6}(2H_0 - 3). \tag{A29}$$

Again Q follows from (34) and phase speed is

$$c = v_0 - W - 1. \tag{A30}$$

APPENDIX B

Summary of Numerical Solution Methods

Numerical integration of (18) and (22) to (25) gives $v_1(x)$, $v_2(x)$, $h(x)$, $\psi_1(x)$, and $p_1(x)$ through use of a fourth-order Taylor expansion of the form

$$f(x_0 + \Delta x) \approx f(x_0) + \Delta x \frac{df}{dx}(x_0) + \frac{\Delta x^2}{2!}\frac{d^2 f}{dx^2}(x_0)$$

$$+ \frac{\Delta x^3}{3!}\frac{d^3 f}{dx^3}(x_0) + \frac{\Delta x^4}{4!}\frac{d^4 f}{dx^4}(x_0) \tag{B1}$$

evaluated at each x level using (18), (22)–(25), and their derivatives. Initially $v_2(x)$ is found by integrating onshore from the shelf edge, then the rest of the solution follows by integrating offshore from the coast. Spacing

Δx is constant except that an extra x level is inserted when an interface outcrop falls between x levels since this marks a change in the nature of the problem from two layers to one layer.

Solutions satisfying the boundary conditions (21) and (26)–(32) are found by an iterative root-finding procedure. When Q is not fixed (e.g., Fig. 8), a value of v_0 must be found for which the boundary condition (26) is satisfied in the ocean. From two initial guesses at v_0 the resulting errors in (26) are used to estimate an improved v_0 for the next iteration. When a specific Q is required (e.g., Figs. 9 and 12), the root-finding procedure has an extra dimension. Values of v_0 and α must be found to match both (26) and the desired Q, requiring three linearly independent initial guesses. These initial guesses can be extrapolated from known solutions with similar parameter values. The analytic curvature-free solution can be used as a starting point from which curvature is increased in small steps toward a desired value.

REFERENCES

Allen, J. S., 1980: Models of wind-driven currents on the continental shelf. *Annu. Rev. Fluid Mech.,* **12,** 389–433.
Barth, J. A., and R. L. Smith, 1998: Separation of a coastal upwelling jet at Cape Blanco, Oregon, USA. *S. Afr. J. Mar. Sci.,* **19,** 5–14.
——, S. D. Pierce, and R. L. Smith, 2000: A separating coastal upwelling jet at Cape Blanco, Oregon, and its connection to the California Current system. *Deep-Sea Res. II,* **47,** 783–810.
Gill, A. E., and E. H. Schumann, 1979: Topographically induced changes in the structure of an inertial coastal jet: Applications to the Agulhas Current. *J. Phys. Oceanogr.,* **9,** 975–991.
Hughes, R. L., 1985a: On inertial currents over a sloping continental shelf. *Dyn. Atmos. Oceans,* **9,** 49–73.
——, 1985b: Multiple criticalities in coastal flows. *Dyn. Atmos. Oceans,* **9,** 321–340.
——, 1989: The hydraulics of local separation in a coastal current with application to the Kuroshio meander. *J. Phys. Oceanogr.,* **19,** 1809–1820.
Huyer, A., E. J. C. Sobey, and R. L. Smith, 1979: The spring transition in currents over the Oregon continental shelf. *J. Geophys. Res.,* **84,** 6995–7011.
Kelly, K. A., 1985: The influence of winds and topography on the sea surface temperature patterns over the Northern California shelf. *J. Geophys. Res.,* **90,** 11 783–11 798.
Long, R. R., 1972: Finite amplitude disturbances in the flow of inviscid rotating and stratified fluids over obstacles. *Annu. Rev. Fluid Mech.,* **4,** 69–92.
Luther, M. E., and J. M. Bane, 1985: Mixed instabilities in the Gulf Stream over the continental slope. *J. Phys. Oceanogr.,* **15,** 3–23.
Mitsudera, H., and R. Grimshaw, 1994: Capture and resonant forcing of solitary waves by the interaction of a baroclinic current with topography. *J. Phys. Oceanogr.,* **24,** 2217–2244.
Ou, H.-S., and P. M. De Ruijter, 1986: Separation of an inertial boundary current from a curved coastline. *J. Phys. Oceanogr.,* **16,** 280–289.
Peffley, M. B., and J. J. O'Brien, 1976: A three-dimensional simulation of coastal upwelling off Oregon. *J. Phys. Oceanogr.,* **6,** 164–180.
Roed, L. P., 1980: Curvature effects on hydraulically driven inertial boundary currents. *J. Fluid Mech.,* **96,** 395–412.
Smith, R. L., 1974: A description of current, wind, and sea level variations during coastal upwelling off the Oregon coast, July–August 1972. *J. Geophys. Res.,* **79,** 435–443.
Woods, A. W., 1988: A study of current structures in a two-layer shelf model. *Dyn. Atmos. Oceans,* **12,** 289–311.